23rd ABCM International Congress of Mechanical Engineering
December 6-11, 2015, Rio de Janeiro, RJ, Brazil

A NUMERICAL ANALYSIS OF BOUNDARY-LAYER/SHOCK WAVE INTERACTIONS IN THE COMPRESSION RAMPS OF SCRAMJET INTAKES

Augusto Fontan Moura[1]
Maurício Antoniazzi Pinheiro Rosa[2]
Instituto de Estudos Avançados, São José dos Campos, Brasil
a.fontanmoura@uq.edu.au
pinheiro@ieav.cta.br

Abstract. *As part of the studies, at the Aerothermodynamics and Hypersonics Division (EAH) of the Institute for Advanced Studies (IEAv), aimed at flight demonstration of a hypersonic vehicle prototype powered by a scramjet engine, a series of numerical simulations have been performed for the inlet of the present vehicle configuration (14-XB) of the 14-X hypersonic vehicle prototype. The aim was to analyze the development of the boundary-layer and its interaction with the shock wave from the compression ramp, which may cause flow separation. First, an analysis is performed on the boundary-layer development at the vehicle forebody, the thickness of which can be considerably large in these flow conditions. Second, a validation study of the transitional viscous flow models and numerical methods available was performed for the simple geometry of a flat plate attached to a compression ramp, compared with similar experimental results from the literature. Results show that the transitional flow models are quite accurate at simulating the flow separation. Finally, a detailed numerical study was performed for the inlet of the 14-XB vehicle, analysing both adiabatic and cold wall conditions, where separation is visible in both, albeit larger for the adiabatic cases. This is invaluable for the development of the engine as these separations alter the flow field in such a way that may lead to engine unstart or adverse conditions at the combustor.*

Keywords: *flow separation, hypersonic flow, compression ramp, numerical simulation*

1. INTRODUCTION

The Aerothermodynamics and Hypersonics Division (EAH) of the Institute for Advanced Studies (IEAv) is conducting a series of studies aimed at flight demonstration of a hypersonic vehicle prototype powered by a scramjet engine. A scramjet (supersonic combustion ramjet) is a variant of a ramjet airbreathing combustion engine in which the fuel combustion process takes place with the incoming compressed air at supersonic speeds. The scramjet is basically composed of three basic components: a converging inlet, where incoming air is compressed and decelerated; a combustor, where gaseous fuel is burned with atmospheric oxygen to produce heat; and a diverging nozzle, where the heated air is accelerated to produce thrust (Segal, 2009; Smart, 2008; Heiser and Pratt, 1994). The design of the inlet is very important as its performance usually dictates the overall performance of the engine (Mahoney, 1990). Due to the corners between compression ramps, it is subject to the presence of shock wave/boundary-layer interactions (SWBLI) responsible for flow separations which may adversely affect the flow field, reducing performance, altering flow properties in the combustor and even leading to engine unstart (Anderson, 1989).

SWBLI happen when a shock wave impinges on a boundary-layer (BL), or is generated from it in a corner, such that it generates an adverse pressure gradient which feeds back through the subsonic portion of the BL, causing flow separation. This generates a series of other shock waves at the flow separation and reattachment points, which interact with each other further downstream to combine into the main ramp shock. At the reattachment point, the BL becomes narrower, leading to an intense temperature gradient that increases heat flux at that point (Anderson, 1989; Brown *et al.*, 2009). SWBLI change the flow structure significantly, affecting engine behavior. An example of SWBLI with all the shock waves it generates is illustrated in Fig. 1.

This paper presents an analysis of the flow at the inlet of the present configuration (14-XB) of the 14-X hypersonic vehicle prototype. It consists of an analysis of BL development in the vehicle forebody for adiabatic and cold wall (fixed wall temperature T_w = 300 K) conditions, followed by a validation of the transitional viscous flow models available using a simple flat plate and compression ramp geometry, comparing with data available in the literature. Finally, an analysis is performed for the inlet of the 14-XB, where flow separation can be observed (Moura, 2014). All simulations were done with the ANSYS Fluent software and the viscous flow models available in it, which will be briefly explained in the next section.

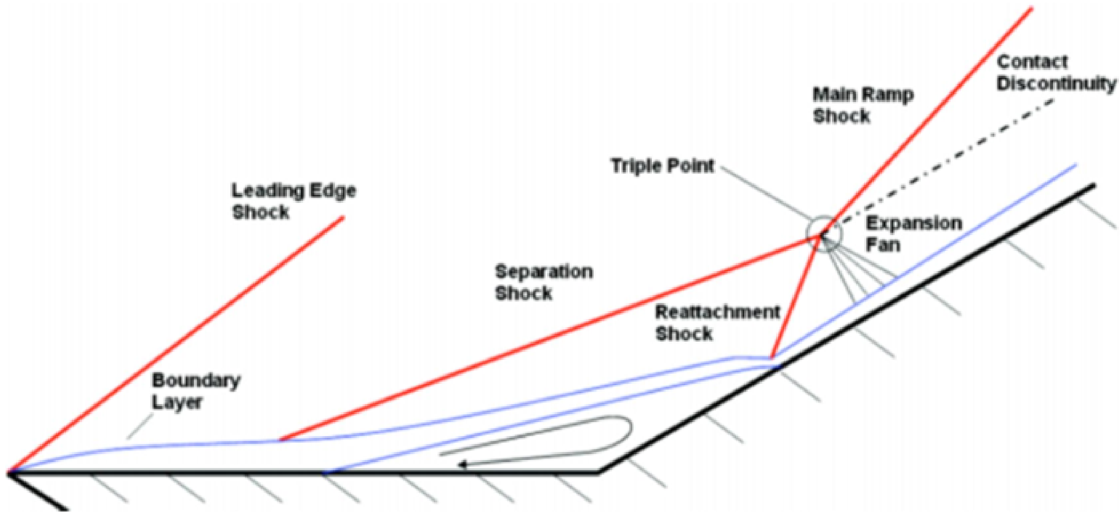

Figure 1. SWBLI-induced flow separation (Brown *et al.*, 2009).

2. METHODOLOGY

In order to calculate the compressible flow in ANSYS Fluent, the RANS equations of continuity (Eq. 1), momentum conservation (Eq. 2) and energy (Eq. 3) are calculated in the form below. In order to close the system of equations, considering air as a calorically perfect gas, it must also be added other expressions for energy (Eq. 4), enthalpy (Eq. 5) and the perfect gas law (Eq. 6):

$$\frac{\delta\rho}{\delta t} + \nabla\cdot(\rho\mathbf{v}) \tag{1}$$

$$\frac{\delta(\rho\mathbf{v}}{\delta t} + \nabla\cdot(\rho\mathbf{v}\mathbf{v}) = -\nabla p + \nabla\overline{\overline{\tau}}_{eff} \tag{2}$$

$$\frac{\delta(\rho E)}{\delta t} + \nabla\cdot[\mathbf{v}(\rho E + p)] = \nabla\cdot[k_{eff}\nabla T + (\overline{\overline{\tau}}_{eff}\cdot\mathbf{v})] \tag{3}$$

$$E = h + \frac{p}{\rho} + \frac{v^2}{2} \tag{4}$$

$$dh = c_p dT \tag{5}$$

$$p = \rho RT \tag{6}$$

where ρ is density, $\mathbf{v}$ is velocity vector, p is pressure, E is total energy, k is thermal conductivity, T is temperature, h is enthalpy, c_p is specific heat at constant pressure and R is the gas constant. The effective viscous stress tensor, $\overline{\overline{\tau}}_{eff}$, is given by Eq. 7:

$$\overline{\overline{\tau}}_{eff} = \mu_{eff}[(\nabla\mathbf{v} + \nabla\mathbf{v}^{\mathbf{T}}) - \frac{2}{3}\nabla\cdot\mathbf{v}I] \tag{7}$$

where I is the unit tensor and μ_{eff} is the effective viscosity. The second term on the right-hand side represents the effect of volume dilation. The subscript eff in Eq. 3 means the effective values, which adds the turbulent term whenever a turbulent model is in use, i.e, $k_{eff} = k_t + k$.

The simulations have been performed with the finite volume density-based solver available in ANSYS Fluent, which solves Eq. 1 to 3 as a coupled set, followed by additional scalars, such as equations for the turbulence models, which are solved independently. The calculations were performed with an implicit approach.

The models used were those available in Fluent for laminar flow, turbulent flow with the Spalart-Allmaras (SA) and SST k-ω models, and transitional flow with the k-kl-ω and Transition SST models, which will be covered briefly here. The Spalart-Allmaras solves a modelled transport equation for the kinematic eddy viscosity and was developed for aerospace applications with wall-bounded flows (Spalart and Allmaras, 1992). The Shear Stress Transport (SST) k-ω blends the accurate formulation of the standard k-ω with the k-ϵ formulation, which is more adequate for the free stream region (Menter, 1994). The k-kl-ω transitional flow model adds a third equation to the turbulent k-ω model, which predicts low-frequency velocity fluctuations in the laminar boundary-layer, which are precursors to transition (Walters and

Cokljat, 2008). Finally, the Transition SST model is a modification of the SST k-ω, coupling it with two more transport equations, one for intermittency and another for the transition onset criteria (Menter *et al.*, 2006).

The analysis begins by simulating the vehicle forebody as a flat plate with length of 500 mm, using as free-stream conditions for the simulation those behind the leading edge oblique shock wave for the nominal flight conditions of Mach 7 at 30 km altitude deflected at 5.5º, i.e. Mach 6.02, $p = 2815$ Pa and $T = 296.7$ K. The analysis includes laminar flow and both turbulent models (SA and SST k-ω), with both adiabatic and cold ($T_w = 300$ K) wall boundary conditions.

Figure 2 shows the geometry used for both the validation of viscous models (L_p =200 mm, $L_r = 210$ mm and $\theta = 15^o$) as well as the analysis of the 14-XB forebody (L_p =657 mm, $L_r = 330$ mm and $\theta = 14.5^o$). For the validation of the viscous flow models, results were compared with experimental (Bleilebens and Olivier, 2006) and CFD (Reinartz *et al.*, 2007) data from the literature. The inflow conditions and details of the mesh used for the validation are given in Tab. 1.

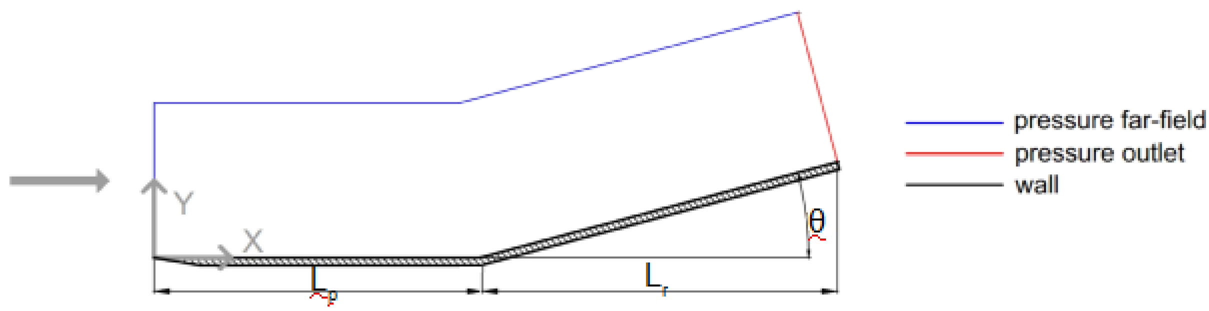

Figure 2. Sketch of the compression ramp case used both in the model validation and the forebody analysis

Table 1. Free-stream flow conditions for the validation study and details of the mesh used (Reinartz *et al.*, 2007). The subscript ∞ indicates free-stream conditions.

M_∞	Re_∞ [10^6/m]	p_∞ [Pa]	u_∞ [m/s]	T_0 [K]	T_∞ [K]	Number of cells			Minimum cell size ratio	
						x	y	Total	x	y
7.42	3.66	2118	2445	2720	265	800	200	160,000	1.5×10^{-5} 1.02	7.5×10^{-5} 1.04

3. RESULTS

To better guarantee the validity of the results for the forebody, a mesh analysis was performed to ensure the solutions were mesh-independent, using two meshes with 123582 and 521485 cells, and results taken for flow properties profiles at several stations along the plate. Results showed good agreement between meshes at all stations, indicating the solution is mesh-independent.

Figure 3 shows velocity and temperature profiles at x = 500 mm for laminar flow with both wall boundary conditions (adiabatic wall and $T_w = 300$ K). It can be seen that the adiabatic case produces much thicker BL, as the increase in temperature mean an increase in viscosity, which in turn means that a larger thickness is necessary for the same velocity gradient. This means the BL is almost three times thicker, which has important implications as these are the conditions the vehicle would face on sustained flight.

Figure 4 shows the results at the same station x = 500 mm with adiabatic wall, this time for the turbulent models in comparison with laminar flow. As can be seen, there isn't much difference between the SA and SST k-ω results, but both present an even thicker BL in comparison with the laminar flow. The laminar BL has lower gradients than the turbulent one, which result in a thicker subsonic region. This is important as a larger subsonic layer increases the propensity of the flow to separate on an SWBLI (Anderson, 1989). These results are important for the analysis of the vehicle inlet as the flow is laminar at the forebody, transitioning downstream in the inlet.

The validation of the viscous models present in ANSYS Fluent was performed by comparing with experimental results from Bleilebens and Olivier (2006) and the FLOWer code CFD data from Reinartz *et al.* (2007) for the geometry shown in Fig. 2. This simple geometry makes it possible to observe flow separation due to SWBLI at the corner where the oblique shock wave from the ramp is generated. The vortex in the separation also induce BL transition in the case of a laminar BL. The case was run with the conditions in Tab. 1 for laminar flow and transitional k-kl-ω and Transition SST models, for a fixed wall temperature $T_w = 819$ K. Results for pressure coefficient and Stanton number at the walls are shown in Fig. 5 along with the results from literature.

In the pressure coefficient results, it can be seen that the laminar flow seems to overpredict the size of the separation

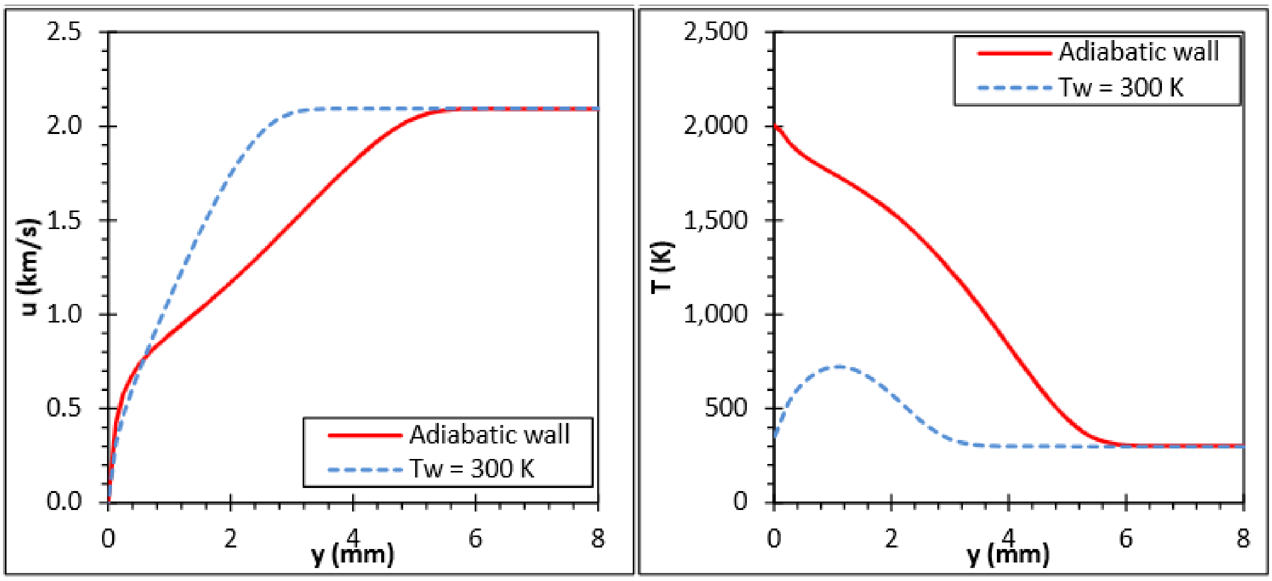

Figure 3. Velocity (left) and temperature (right) profiles at x = 500 mm for laminar flow over a flat plate with adiabatic wall and $T_w = 300$ K

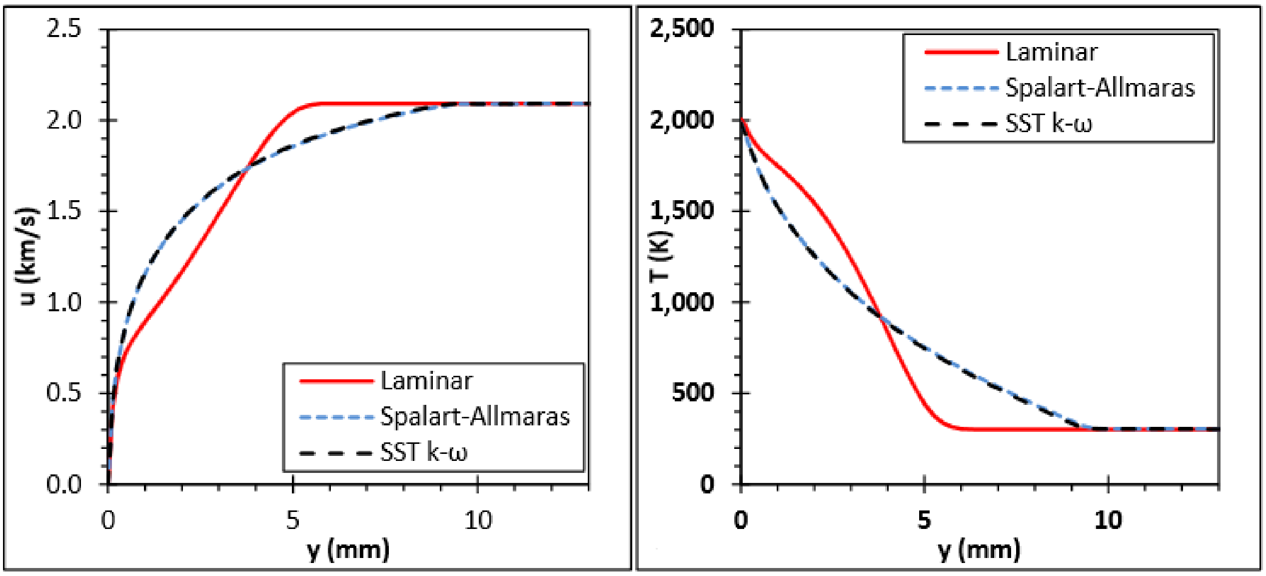

Figure 4. Velocity (left) and temperature (right) profiles at x = 500 mm for laminar and turbulent flow over a flat plate with adiabatic wall

region, both in comparison with the CFD data from the FLOWer code and the experimental data. This happens because the flow actually transitions to turbulence due to the separation, limiting its length. In the case of the FLOWer code, Reinartz *et al.* (2007), used a trip to transition the flow at the corner, so it doesn't actually calculate transition but rather imposes it into the flow. A comment must be made on the oscillations seen in the laminar results, which are due to instabilities in the separation. The separation region houses vortices which are inherently 3D and not very well solved by the 2D simulations, as well as unsteady phenomena in the oscillation of the separation shock wave (Lee and Wang, 1995). Therefore, results for laminar flow are unstable and the solution tends to diverge as the separation region starts increasing to take over the domain. As such, these results were obtained by comparing the results along the initial flat plate for those of a single flat pate, in order to determine the correct development of the BL and ensure the separation region is properly solved.

For the transitional flow models, it can be seen that the k-kl-ω model is able to accurately predict the length of the separation region, agreeing well with both experiment and CFD up to the peak after the corner. At this point, it actually presents better agreement with the experimental results than the FLOWer code data. The Transition SST model, on the other hand, underpredicts the length of separation and, as a consequence, the pressure increase after the shock wave. On the other hand, for the Stanton number results, it can be seen that the Transition SST better predicts the peak values at reattachment, agreeing with the experimental data downstream from the corner. The k-kl-ω model, on the other hand, reaches a much lower value at the reattachment, increasing only further downstream to match the Transition SST results.

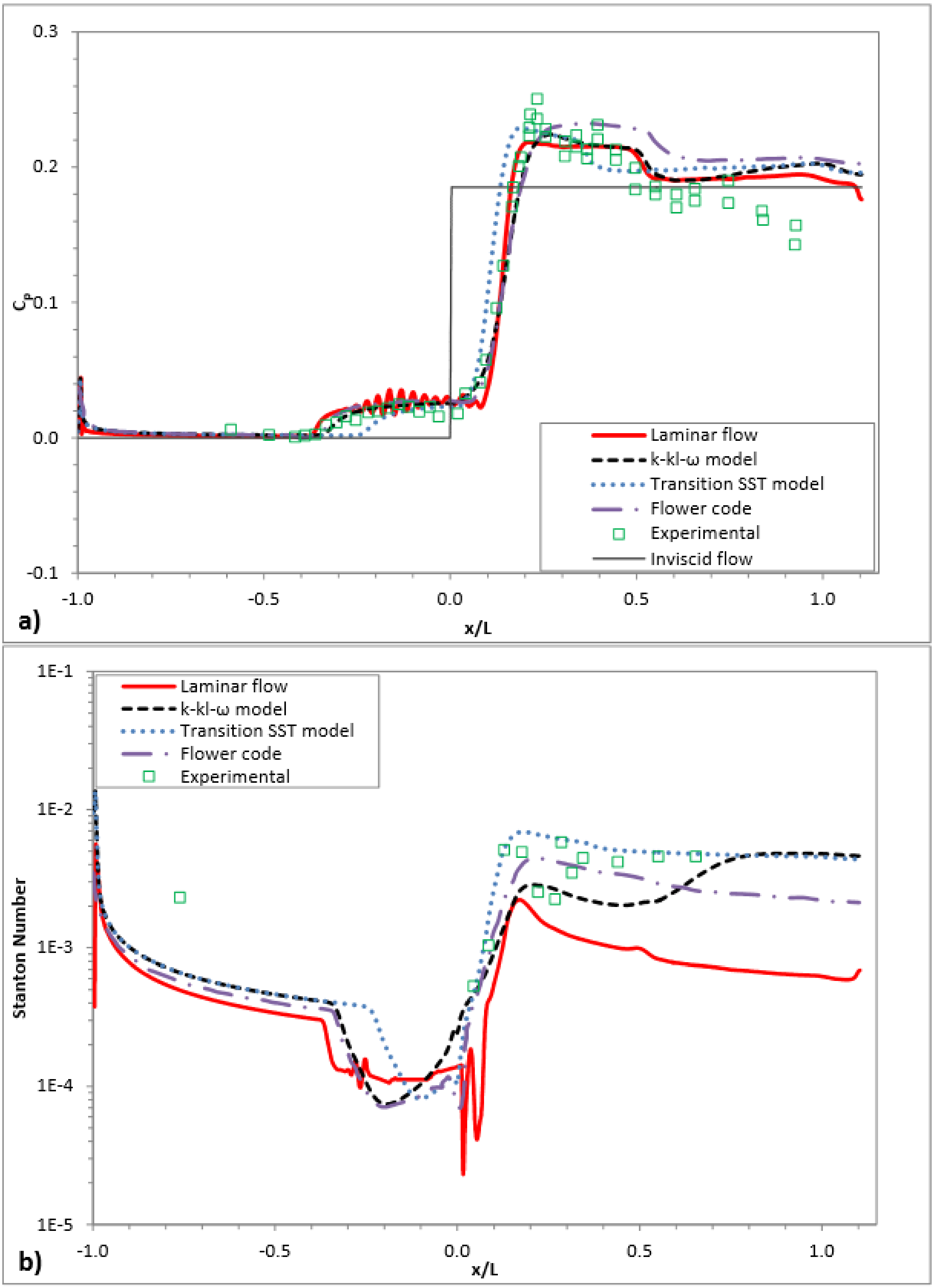

Figure 5. a) pressure coefficient and b) Stanton number results for laminar flow and transitional models k-kl-ω and Transition SST in comparison with experimental (Bleilebens and Olivier, 2006) and CFD (Reinartz *et al.*, 2007) data.

The FLOWer code results sit between these two, agreeing only with the k-kl-ω model in the length of the separation. This shows that, while neither model is capable of accurately representing the entire flow field, they are both accurate at certain regions so that the k-kl-ω model could be used to calculate the separation region and the flow structures of the shock waves generated, while the Transition SST could be used to properly calculate the heat transfer at the walls around the separation.

Figure 6 shows the Mach number contours for the transitional flow models. Here it can be clearly seen the difference in separation length between the models, as observed in the plots in Fig. 5. With these results and the knowledge of the capabilities and limitations of the models available in ANSYS Fluent, an analysis of the part of the inlet of the 14-XB hypersonic vehicle is performed in the same way as the validation study, by setting the forebody as a flat plate with the second compression ramp attached, using as inlet conditions the flow behind of the leading edge shock wave, the same used for the forebody analysis.

Figure 7 shows the pressure coefficient for both adiabatic wall and T_w = 300 K, and the Stanton number for Tw = 300 K for both transitional models and the SA turbulence model. As seen in the validation results, the separation region is bigger for the k-kl-ω model in relation to the Transition SST, while the SA model shows no separation region, as is expected for the turbulent flow. This is important, as turbulence may be induced at the forebody, for example with a step or trip, so that no separation will occur at the corner for the nominal flight condition of the 14-XB. As for the Stanton number results, they clearly show that the flow transitions after the separation, with the values for both transitional models reaching the same as for the SA after the corner. The Transition SST model again shows a higher peak, actually above the SA model, which is where reattachment occurs and the BL gets narrower, increasing heat flux.

Figure 8 shows the Mach number contours at the corner region for the adiabatic wall condition. The separation can be clearly seen, along with the separation shock and a strong reattachment shock. The separation region is considerably large for the adiabatic case, occupying up to 30% of the forebody of the vehicle.

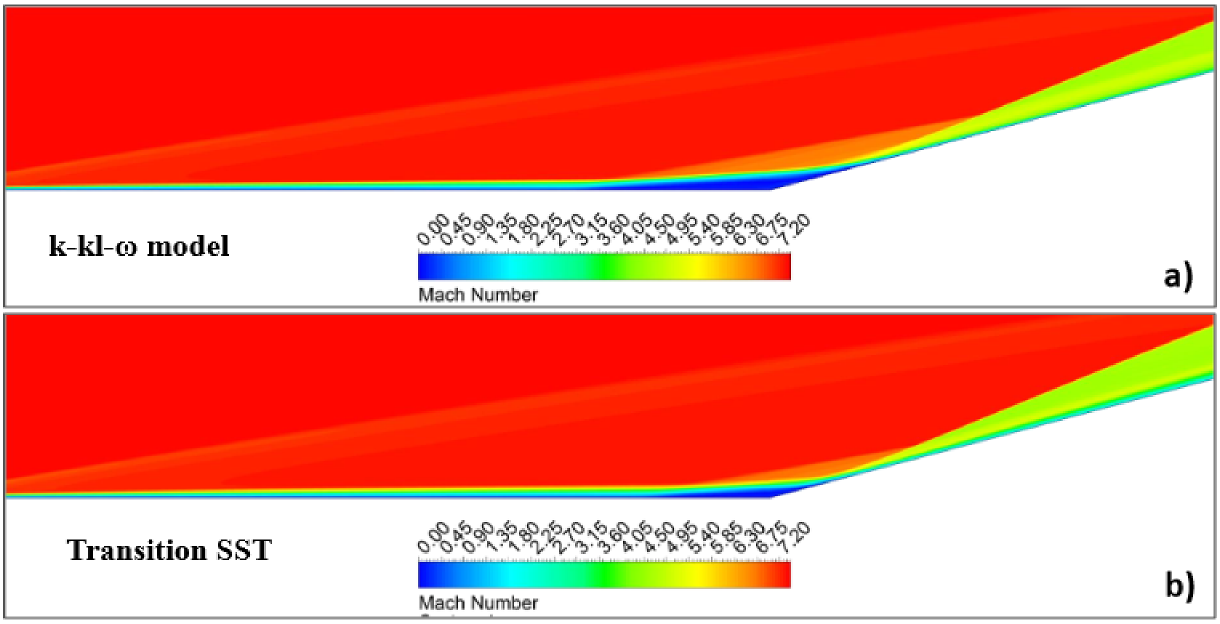

Figure 6. Mach number contours for a)k-kl-ω and b) Transition SST models for Condition II, $T_w = 819$ K

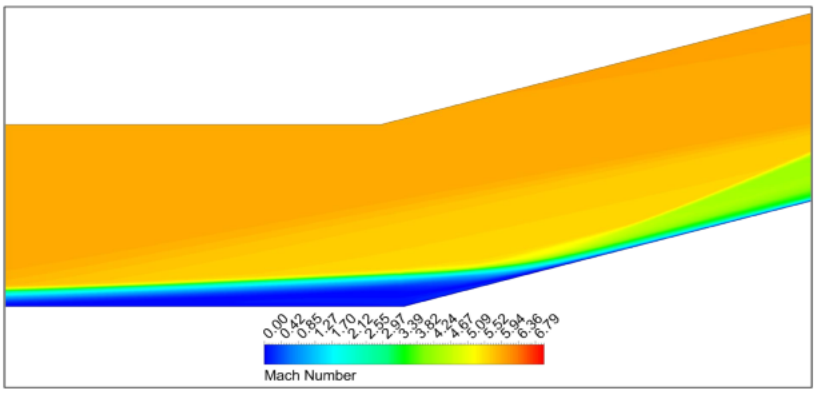

Figure 8. Mach number contours for the 14-XB inlet with the k-kl-ω model and adiabatic wall condition

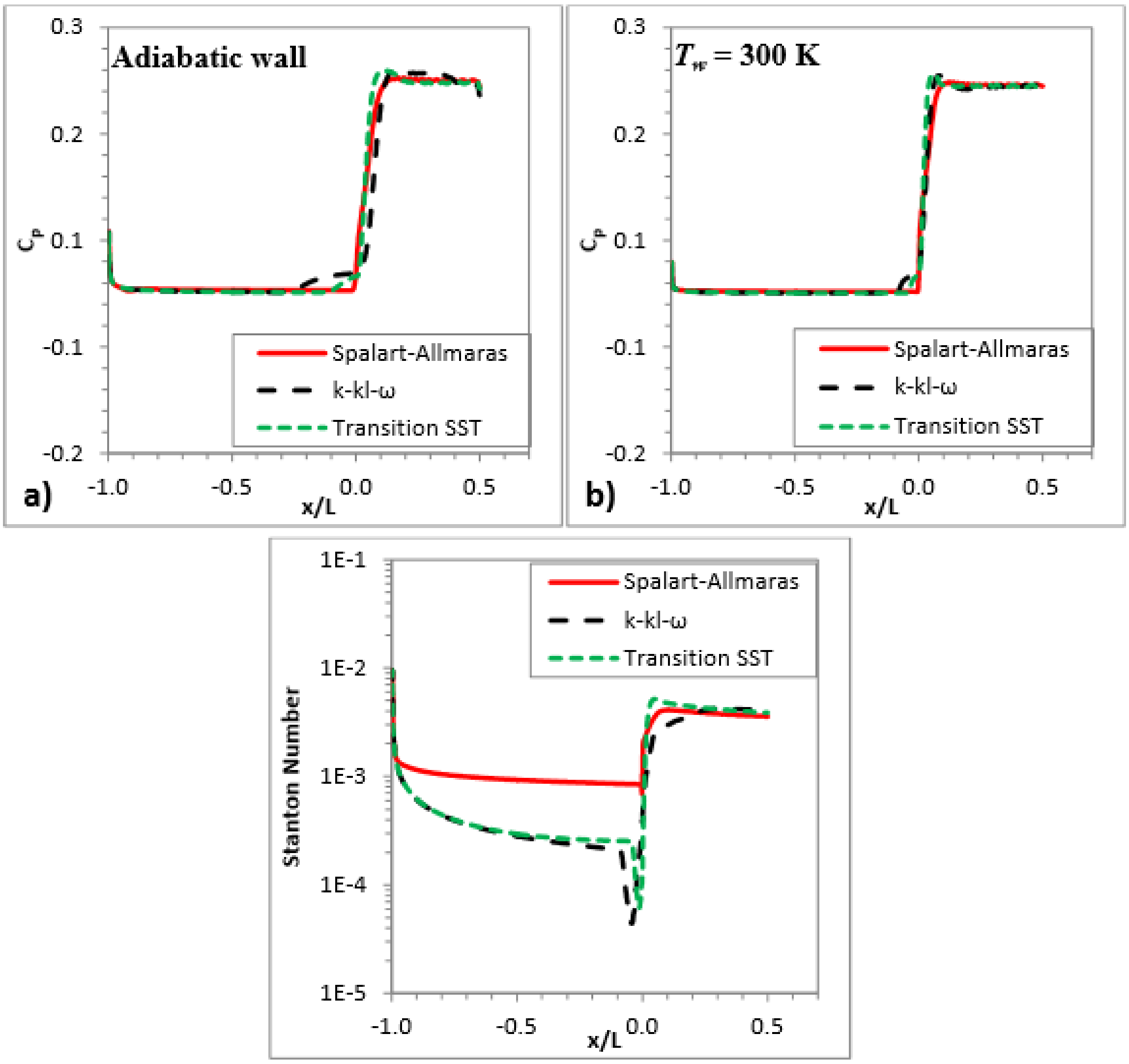

Figure 7. Pressure coefficient for a) adiabatic wall and b) $T_w = 300$ K, and c) Stanton number for $T_w = 300$ K with the k-kl-ω, Transition SST and SA models for the 14-XB inlet

4. CONCLUSION

First of all, results indicate that the transitional models available in ANSYS Fluent are adequate, albeit not perfect each on its own, for the calculation of the SWBLI and flow separation for the hypersonic flight conditions of the 14-XB. This gives more confidence in the results obtained for both the forebody alone and the partial inlet with forebody and compression ramp. The former indicate that boundary-layers can get quite thick in the forebody of the vehicle, which can lead to separation. The inlet results, on the other hand, show that there is indeed separation at the corner between the ramps, and that this separation promotes boundary-layer transition, which becomes turbulent downstream of the corner. These results are important for the vehicle design as the presence of the separation region alters the shock waves and the flow structure at the inlet causing it to operate outside its design conditions so that its performance may be adversely affected. Future work includes the simulation of the entire inlet and combustor, as the shock wave reflection on the cowl can produce another separation at the throat region of the engine; run an experimental campaign of the inlet geometry to directly compare the results obtained in this thesis; simulate a step or trip to force transition to turbulence and avoid the separation due to SWBLI; analyze the effects of a blunt leading edge, among others.

5. ACKNOWLEDGEMENTS

The authors would like to acknowledge CNPq for the financial support provided to project number 560143/2010-9.

6. REFERENCES

Anderson, J.D., 1989. *Hypersonics and High Temperature Gas Dynamics*. McGraw-Hill, New York, 1st edition.

Bleilebens, M. and Olivier, H., 2006. "On the influence of elevated surface temperatures on hypersonic shock wave/boundary layer interaction at a heated ramp model". *Shock Waves*, Vol. 15, No. 5, pp. 301–312. ISSN 0938-1287. doi:10.1007/s00193-006-0025-2. URL `http://link.springer.com/10.1007/s00193-006-0025-2`.

Brown, L.M., Boyce, R.R., Mudford, N. and O'Byrne, S., 2009. "Intrinsic three-dimensionality of laminar hypersonic shock wave/boundary layer interactions". *AIAA 2009-7205*, pp. 1–17. URL `http://arc.aiaa.org/doi/pdf/10.2514/6.2009-7205`.

Heiser, W. and Pratt, D., 1994. *Hypersonic Airbreathing Propulsion*. Number pt. 1 in AIAA Textbooks Series. American Institute of Aeronautics and Astronautics. ISBN 9781563470356. URL `https://books.google.com.au/books?id=d1sQvT2_kMsC`.

Lee, C. and Wang, S., 1995. "Study of the shock motion in a hypersonic shock system/turbulent boundary layer interaction". *Experiments in Fluids*, Vol. 19, No. 3, pp. 143–149. ISSN 0723-4864. doi:10.1007/BF00189702. URL `http://dx.doi.org/10.1007/BF00189702`.

Mahoney, J.J., 1990. *Inlets for Supersonic Missiles*. AIAA Education Series, Washington, DC, 1st edition.

Menter, F.R., 1994. "Two-equation eddy-viscosity turbulence models for engineering applications". *AIAA Journal*, Vol. 32, No. 8, pp. 1598–1605. ISSN 0001-1452. doi:10.2514/3.12149. URL `http://arc.aiaa.org/doi/abs/10.2514/3.12149`.

Menter, F.R., Langtry, R.B., Likki, S.R., Suzen, Y.B., Huang, P.G. and Volker, S., 2006. "A Correlation-Based Transition Model Using Local Variables—Part I: Model Formulation". *Journal of Turbomachinery*, Vol. 128, No. 3, p. 413. ISSN 0889504X. doi:10.1115/1.2184352. URL `http://turbomachinery.asmedigitalcollection.asme.org/article.aspx?articleid=1467239`.

Moura, A.F., 2014. *A computational study of the airflow in scramjet intakes*. Master's thesis, Instituto Tecnológico de Aeronáutica, São José dos Campos, Brazil.

Reinartz, B., Ballmann, J., Brown, L., Fischer, C. and Boyce, R.R., 2007. "Shock wave/boundary layer interaction in hypersonic intake flows". *2nd European Conference for Aerospace Sciences*, pp. 1–8. URL `http://www.cats.rwth-aachen.de:8080/ reinartz/literature/Reinartz_EUCASS_2007.pdf`.

Segal, C., 2009. *The Scramjet Engine: Processes and Characteristics*. Cambridge University Press, Cambridge, 1st edition. ISBN 9780521838153.

Smart, M., 2008. "Scramjets". *RTO-EN-AVT-150*, pp. 1–38.

Spalart, P. and Allmaras, S., 1992. "A one-equation turbulence model for aerodynamic flows". *AIAA-92-G439*. URL `http://arc.aiaa.org/doi/pdf/10.2514/6.1992-439`.

Walters, D.K. and Cokljat, D., 2008. "A Three-Equation Eddy-Viscosity Model for Reynolds-Averaged Navier–Stokes Simulations of Transitional Flow". *Journal of Fluids Engineering*, Vol. 130, No. 12, p. 121401. ISSN 00982202. doi:10.1115/1.2979230. URL `http://fluidsengineering.asmedigitalcollection.asme.org/article.aspx?articleid=1478203`.

7. RESPONSIBILITY NOTICE

The authors are the only responsibles for the printed material included in this paper.